MPP-2007-19

Neutrino mass from future high redshift galaxy surveys: sensitivity and detection threshold

Steen Hannestad

Department of Physics and Astronomy
University of Aarhus, DK-8000 Aarhus C, Denmark

Yvonne Y. Y. Wong

Max-Planck-Institut für Physik (Werner-Heisenberg-Institut)
Föhringer Ring 6, D-80805 München, Germany

E-mail: sth@phys.au.dk,ywong@mppmu.mpg.de

Abstract. We calculate the sensitivity of future cosmic microwave background probes and large scale structure measurements from galaxy redshift surveys to the neutrino mass. We find that, for minimal models with few parameters, a measurement of the matter power spectrum over a large range of redshifts has more constraining power than a single measurement at low redshifts. However, this improvement in sensitivity does not extend to larger models. We also quantify how the non-Gaussian nature of the posterior distribution function with respect to the individual cosmological parameter influences such quantities as the sensitivity and the detection threshold. For realistic assumptions about future large scale structure data, the minimum detectable neutrino mass at 95 % C.L. is about 0.05 eV in the context of a minimal 8-parameter cosmological model. In a more general model framework, however, the detection threshold can increase by as much as a factor of three.

1. Introduction

Neutrinos differ from other types of energy density content in our universe in two significant ways: They are essentially non-interacting during the entire epoch of structure formation, and transit from a relativistic to a non-relativistic particle species also in the same epoch. The first aspect means that the dynamics of neutrinos cannot be described by simple fluid equations; effectively, the neutrino fluid has infinite viscosity. The second aspect means that neutrinos free-stream a finite distance before becoming non-relativistic; this introduces a new scale, the neutrino free-streaming scale.

These unique features imply that cosmology can be used as a very efficient tool to constrain the neutrino mass. For neutrinos of sub-eV masses, the signature of massive neutrinos on the large scale structure (LSS) power spectrum, i.e., the gradual damping of fluctuation power, falls between wavenumbers $k \sim 0.01\ h\ \mathrm{Mpc}^{-1}$ and $0.5\ h\ \mathrm{Mpc}^{-1}$, a range conveniently probed by current cosmological probes. Indeed, shape information from presently available measurements of the LSS power spectrum, when combined with observations of the cosmic microwave background (CMB) anisotropies, can already constrain the upper limit on the sum of all neutrino mass eigenstates $\sum m_\nu$ to lie in the range $0.2 \rightarrow 1$ eV in the context of the concordance ΛCDM model. The precise value of the limit depends strongly on the data sets used, as well as on the number of free cosmological parameters employed in the analysis (see [1–10] for a selection of recent papers on the subject).

Furthermore, because the fraction of highly non-relativistic neutrinos changes with time, and only highly non-relativistic neutrinos can cluster, the impact of neutrinos on structure formation depends not only on scale, but also on time. For neutrinos that are non-relativistic today, the LSS power spectrum in terms of wavenumber k and redshift z is approximately given by [11]

$$P(k,z) = P_{\mathrm{CDM}}(k,0) \times \begin{cases} \left(\dfrac{g(z)}{(1+z)g(0)}\right)^2 & k < k_{\mathrm{fs}} \\ \left(\dfrac{g(z)}{(1+z)g(0)}\right)^{2-6f_\nu/5} (1-f_\nu)^3 [g(0)/a_{\mathrm{nr}}]^{-6f_\nu/5} & k > k_{\mathrm{fs}} \end{cases}, \tag{1.1}$$

where $f_\nu = \Omega_\nu/\Omega_m$, $a_{\mathrm{nr}} = a(m_\nu = 3T_\nu)$ is the scale factor at which neutrinos become non-relativistic, and $g(z)$ quantifies the decay rate of the gravitational potential. Save for the case of $\Omega_{\mathrm{total}} = \Omega_m = 1$, $g(z)$ is a time-dependent function, so that the power spectrum suppression due to neutrino free-streaming on scales below the free-streaming length $\lambda_{\mathrm{fs}} = 2\pi/k_{\mathrm{fs}}$ is also time-dependent. Figure 1 shows the suppression in the case of $\sum m_\nu = 0.08$ eV relative to $\sum m_\nu = 0$ eV as a function of k and z. On large scales the two spectra are identical, while on small scales the suppression matches equation (1.1). The rapid oscillations in $P(k,z)/P_{m_\nu=0}(k,z)$ can be attributed to baryon acoustic oscillations (BAO) in the power spectra.

Clearly, cosmological probes that tap the power spectrum information in terms of

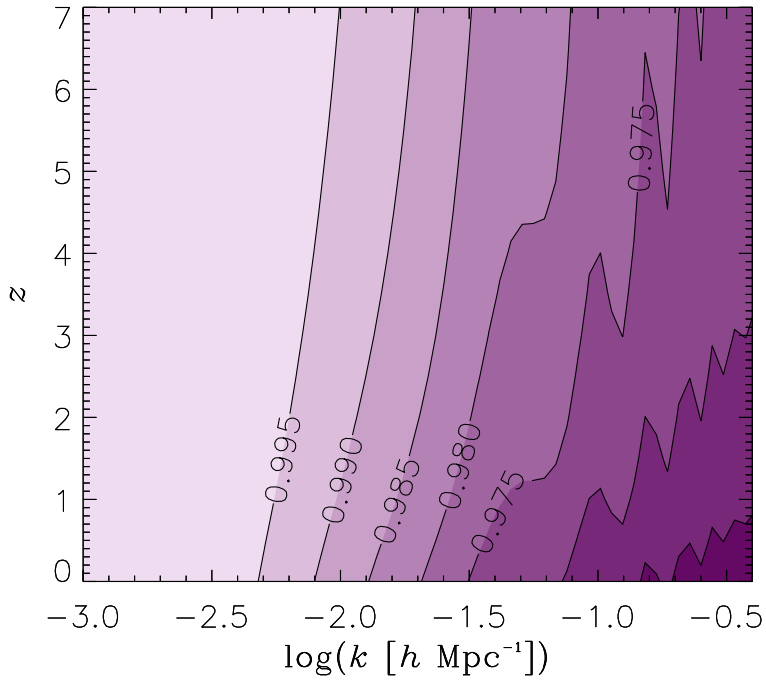

Figure 1. The power spectrum suppression factor $P(k,z)/P_{m_\nu=0}(k,z)$ as a function of wavenumber k and redshift z for a neutrino mass of $\sum m_\nu = 0.08$ eV. The shadings are from 0.96 (darkest) to 1.00 (lightest) in steps of 0.005.

both the wavenumber k and the redshift z are *a priori* extremely sensitive to the neutrino mass. One notable example is weak gravitational lensing of distant galaxies, for which the impact of massive neutrinos has been studied extensively (see, e.g., [12–15]).

Another example is high-redshift galaxy surveys. The power of combining CMB data with LSS measurements from low-redshift galaxy surveys to probe neutrino masses has, since the pioneering work of [16], been discussed in many previous studies (see, e.g., [17, 18]). In contrast, the advantage of using combinations of both low- and high-redshift surveys has, apart from the study of [19], received relatively little attention so far.

The purpose of the present paper is to explore this last possibility in detail. A number of high-redshift galaxy surveys have been proposed for the next decade and beyond. The Wide Field Multiple Object Spectrograph (WFMOS) survey proposed for the Subaru 8m telescope, for example, plans to observe at redshifts $z \sim 1$ and $z \sim 3$ [20]. The Hobby-Eberly Telescope Dark Energy Experiment (HETDEX) will similarly look out to $z \sim 4$ [21]. Further down in time, the Cosmic Inflation Probe (CIP) mission will observe at even higher redshifts in space [22].

For simplicity we will adopt the survey set-ups used in [19]. However, our analysis differs from [19] in several important ways: (i) We use a simulation-based method for our parameter error forecast, which has been shown to have many advantages over the popular Fisher matrix approach [23]. (ii) We derive our constraints within more general cosmological frameworks that include uncertainties in, e.g., dark energy equation of state, and other parameters degenerate with the neutrino mass. This has

important implications for the sensitivity to $\sum m_\nu$ and its detection threshold. (iii) We opt to work with spherically-averaged, one-dimensional power spectra, instead of two-dimensional spectra which in principle contain additional information from geometrical and redshift-space distortions. However, in contrast to the smoothed spectrum analysis of [19], we include also information from baryon acoustic oscillations. Combination of geometrical/redshift effects and BAO will likely lead to even more powerful parameter constraints [24, 25]. (iv) Several consistent assumptions in [19], particularly in the calculation of the CMB anisotropies, are rectified.

Lastly, let us note that, aside from the ability to probe the power spectrum evolution, going to high redshifts has the advantage of reducing nonlinearities. At low redshifts ($z < 0.5$), uncertainties in the power spectrum in the nonlinear regime require that we restrict the use of galaxy survey data to wavenumbers not exceeding $k \sim 0.1\ h\ \mathrm{Mpc}^{-1}$. Indeed, for neutrino masses below 0.1 eV, the effects of nonlinearity are already comparable to the damping of fluctuation power due to neutrino free-streaming on scales around $0.05\ h\ \mathrm{Mpc}^{-1}$ at $z = 0$. At higher redshifts, however, nonlinear effects are less prominent, and it is possible to probe safely the LSS power spectrum at much larger values of k. This simple fact has important consequences for constraints on neutrino masses.

2. Parameter error forecast

We use a simulation-based method to estimate cosmological parameter errors from various combinations of future CMB and galaxy redshift surveys. Synthetic data are generated according to the experimental specifications of the cosmological probe of interest, and then analysed using a Markov Chain Monte Carlo (MCMC) package such as CosmoMC [26, 27]. The many advantages of MCMC-based forecasts over the popular Fisher matrix approach are discussed in detail in [23]. Here, it suffices to reiterate that the MCMC method, which probes the entire likelihood hypersurface, generally provides more reliable results than does a Fisher matrix analysis based on estimating the likelihood curvature around the best-fit point.

Reference [23] describes in detail an MCMC parameter forecast using synthetic CMB data. We extend the analysis to include also synthetic LSS data from galaxy redshift surveys as follows.

2.1. Galaxy power spectrum

Galaxy redshift surveys measure the correlation spectrum of galaxy number density fluctuations, $P_g(k)$. In turn, this correlation spectrum is related to the underlying matter power spectrum $P(k)$ via

$$P_g(k) = b^2 P(k), \tag{2.1}$$

where the bias parameter b varies according to the galaxy type targeted by the survey at hand, but is generally expected to be independent of k in the linear regime.

Table 1. Mock galaxy survey specifications. From left to right, z_c is the central redshift of each survey slice, $k_{\rm min}$ ($k_{\rm max}$) the minimum (maximum) wavenumber probed by the slice, $V_{\rm eff}$ the slice's effective volume, $\bar{n}_g$ the comoving number density of galaxies, and b the bias factor. See [19] for a discussion of the calculation of b.

Survey	z_c	$k_{\rm min}$ $[10^{-3}\ h\ {\rm Mpc}^{-1}]$	$k_{\rm max}$ $[h\ {\rm Mpc}^{-1}]$	$V_{\rm eff}$ $[h^{-3}\ {\rm Gpc}^3]$	$\bar{n}_g$ $[10^{-3}h^3\ {\rm Mpc}^{-3}]$	b
G1	0.75	5.32	0.14	1.65	0.5	1.22
$(0.5 < z < 2)$	1.25	4.54	0.19	2.65	0.5	1.47
	1.75	4.26	0.25	3.20	0.5	1.75
G2	2.25	7.15	0.32	0.68	0.5	2.03
$(2 < z < 4)$	2.75	7.11	0.41	0.69	0.5	2.32
	3.25	7.18	0.52	0.67	0.5	2.62
	3.75	7.29	0.64	0.64	0.5	2.92
SG	4	5.82	0.71	1.26	5	4
$(4 < z < 6)$	5	6.03	1.01	1.13	5	5
	6	6.24	1.50	1.02	5	5.5

Given some survey design and restricting the analysis to the linear regime, one can expect to measure the galaxy power spectrum $P_g(k)$ at a range of wavenumbers $k \in [k_{\rm min}, k_{\rm max}]$ up to a statistical uncertainty of [28]

$$\Delta P_g(k) = \sqrt{\frac{1}{2\pi\ w(k)\ \Delta \ln k}} \left[P_g(k) + \frac{1}{\bar{n}_g} \right]. \tag{2.2}$$

Here, $w(k) = (k/2\pi)^3\ V_{\rm eff}$, and

$$V_{\rm eff} = \int d^3r\ \left[\frac{\bar{n}_g(\boldsymbol{r}) P_g(k)}{1 + \bar{n}_g(\boldsymbol{r}) P_g(k)} \right]^2 \tag{2.3}$$

is the effective volume of the survey, with $\bar{n}_g(\boldsymbol{r})$ the expectation value of the galaxy number density at coordinate $\boldsymbol{r}$. When the condition $\bar{n}_g P_g(k) \gg 1$ holds, $V_{\rm eff}$ is equivalent to the actual volume of the survey.

The quantity $\Delta \ln k$ is the bin size at k in $\ln k$-space. In general we use a very fine binning scheme to capture as much of the features in $P_g(k)$ as possible, including wiggles from baryon acoustic oscillations (BAO) at $k \gtrsim 0.01\ {\rm Mpc}^{-1}$. The effect of smearing due to finite window functions, and hence a partial loss of the BAO features in a realistically reconstructed power spectrum, will be discussed in section 2.4.

2.2. Mock survey parameters

Following [19], we consider galaxy surveys probing three different ranges of redshifts:

- G1: $0.5 < z < 2$, ground-based, $\Omega_{\rm sky} = 1500\ {\rm deg}^2$,
- G2 : $2 < z < 4$, ground-based, $\Omega_{\rm sky} = 300\ {\rm deg}^2$, and
- SG : $4 < z < 6$, space-based, $\Omega_{\rm sky} = 300\ {\rm deg}^2$,

where $\Omega_{\rm sky}$ denotes the survey's sky coverage. Note that our G1 survey has five times the sky coverage (and hence survey volume) of the survey of the same name in [19]. We further subdivide each survey by redshift, although we have also checked that, within our one-dimensional (i.e., spherically-averaged spectrum) approach, subdivision or not makes essentially no difference to the final results. Table 1 shows the central redshift z_c, effective volume $V_{\rm eff}$, and other specifications for each of these mock surveys and their subvisions. As a rough guideline, the specifications of G1 are similar to those of the $z \sim 1$ WFMOS survey [20], while G2 is akin to HETDEX [21] or the $z \sim 3$ WFMOS survey [20]. The space-based survey SG should be a reasonable approximation of CIP [22]. See [19] for a more detailed discussion.

Note that the range of wavenumbers probed varies from survey to survey, and, indeed, from redshift slice to redshift slice. At the low end of the spectrum, the slice/survey volume defines the minimum wavenumber $k_{\rm min}$ available for observation,

$$k_{\rm min} = 2\pi/V_{\rm eff}^{1/3}, \tag{2.4}$$

so that the largest observable perturbation wavelength does not exceed the slice's effective length scale. At the other extreme, the maximum wavenumber $k_{\rm max}$ is chosen according to the criterion that the dimensionless power spectrum,

$$\Delta^2(k) \equiv \frac{k^3 P(k)}{2\pi^2}, \tag{2.5}$$

does not exceed unity in the linear theory. Rather than setting common $k_{\rm min}$ and $k_{\rm max}$ for all surveys/slices of interest, we choose to adhere to these "natural" limits, because the (in)ability to probe higher wavenumbers at (low) high redshifts, or the (in)availability of smaller k-modes in (small) large survey volumes reveal the true strengths and drawbacks of each survey set-up.

2.3. Mock data and the likelihood function

The first step of an MCMC forecast consists of generating a vector of N observed data points

$$\boldsymbol{d} = \left(\ P_g^{\rm obs}(k_1), \ \ \cdots, \ \ P_g^{\rm obs}(k_N) \ \right)^T, \tag{2.6}$$

and the corresponding error covariance matrix

$$\boldsymbol{N} = {\rm diag}\left(\ [\Delta P_g(k_1)]^2, \ \ \cdots, \ \ [\Delta P_g(k_N)]^2 \ \right), \tag{2.7}$$

for a given fiducial model and survey/slice. For simplicity, we take the data points $P_g^{\rm obs}(k_i)$ to be equal to the fiducial power spectrum $P_g^{\rm fid}(k_i)$, with errors given by equation (2.2). A more rigorous analysis would require that we draw a random $P_g^{\rm obs}(k_i)$ from a Gaussian centered on $P_g^{\rm fid}(k_i)$ with variance $[\Delta P_g(k_i)]^2$ at every k_i.

Since both the signal and noise are Gaussian-distributed, we can construct a likelihood function in the form

$$L \propto \exp\left[-\frac{1}{2} (b^2 \boldsymbol{v} - \boldsymbol{d})^T \boldsymbol{N}^{-1} (b^2 \boldsymbol{v} - \boldsymbol{d}) \right], \tag{2.8}$$

where the vector $\boldsymbol{v}$,

$$\boldsymbol{v} = \Big(\; P^{\rm th}(k_1), \;\; \cdots, \;\; P^{\rm th}(k_N) \; \Big)^T, \tag{2.9}$$

denotes theoretical predictions of the matter power spectrum $P(k)$. Since the N data points are assumed to be uncorrelated, the likelihood function is equivalent to

$$\chi^2 \equiv -2 \ln L = \sum_i^N \left[\frac{P_g^{\rm obs}(k_i) - b^2 P^{\rm th}(k_i)}{\Delta P_g(k_i)} \right]^2, \tag{2.10}$$

up to a constant offset.

Observe how the bias parameter b enters the likelihood function (2.8). In general we are not interested in the exact value of b; instead, we construct an effective likelihood function $L_{\rm eff}$ by marginalising over b^2,

$$L_{\rm eff} \propto \int db^2 \; \pi(b^2) \; L. \tag{2.11}$$

If the prior $\pi(b^2)$ is flat, the marginalisation can be performed analytically to give

$$\begin{aligned} \chi^2_{\rm eff} &\equiv \; -2 \ln L_{\rm eff} \\ &= \boldsymbol{d}^T \left(\boldsymbol{N}^{-1} - \frac{\boldsymbol{N}^{-1} \boldsymbol{v} \boldsymbol{v}^T \boldsymbol{N}^{-1}}{\boldsymbol{v}^T \boldsymbol{N}^{-1} \boldsymbol{v}} \right) \boldsymbol{d} + \ln(\boldsymbol{v}^T \boldsymbol{N}^{-1} \boldsymbol{v}), \end{aligned} \tag{2.12}$$

again, up to a constant offset.

For multiple surveys/slices, the combined likelihood is simply a product of the individual effective likelihood functions. The CMB likelihood can be also be incorporated in a similar fashion.

2.4. Window functions

Our treatment so far supposes that the power spectrum, including the BAO wiggles, is well-sampled. In reality, however, the finite widths of the window functions used in the reconstruction of the power spectrum from a galaxy survey will smear out the power in Fourier space, so that little of the BAO features remain in the reconstructed spectrum; A separate analysis in terms of real space two-point correlation must be performed in order to extract the BAO peak.

It is interesting to compare the sensitivities of future galaxy redshift surveys both with and without BAO extraction. As said, the former case is already covered by our default treatment. For the latter case, we mimic the effect of a finite window function by smoothing the fiducial power spectrum with a normalised top-hat function in log space,

$$\ln P_g^{\rm sm}(k) = \int d \ln k' \; W(k, k', R) \; \ln P_g(k'), \tag{2.13}$$

where

$$W(k, k', R) = \begin{cases} 1/R, & \ln k - R/2 \leq \ln k' \leq \ln k + R/2, \\ 0, & \text{otherwise.} \end{cases} \tag{2.14}$$

We use $R = 0.33$, roughly similar to the "1σ" width of the SDSS LRG window functions [29]. Mock data points are then drawn from the smoothed spectrum $P_g^{\rm sm}(k)$ with errors given by (2.2).

2.5. Mock CMB data

Since the LSS power spectrum is generally fairly featureless, parameter degeneracies abound so that measurements from galaxy redshift surveys alone do not place very stringent limits on cosmological parameters. In order to break these degeneracies, it is common to consider power spectrum measurements together with data from CMB observations. In the present work, we consider prospective CMB data from the Planck satellite [30]. We assume measurements of the auto and cross correlation power spectra of the CMB temperature and E-type polarisation (i.e., TT, TE, EE), up to a multipole $\ell = 2250$. Experimental characteristics of the Planck satellite, assuming one year of observation, can be found in Table 1.1 of the Planck Bluebook [31].

2.6. Fiducial models

We consider two spatially flat cosmological models with eight and ten parameters respectively,

$$\begin{aligned} \boldsymbol{\Theta}_8 &= \{\omega_b, \omega_c, \sum m_\nu, N_\nu, h, \tau, A_s, n_s\}, \\ \boldsymbol{\Theta}_{10} &= \{\omega_b, \omega_c, \sum m_\nu, N_\nu, h, \tau, A_s, n_s, \alpha_s, w\}, \end{aligned} \tag{2.15}$$

where $\omega_b \equiv \Omega_b h^2 = 0.0223$ is the baryon density, $\omega_c \equiv \Omega_c h^2 = 0.105$ the cold dark matter density, $\sum m_\nu = 0$ the sum of neutrino masses, $N_\nu = 3.04$ the effective number of fermionic degrees of freedom during radiation domination, $h = 0.7$ the Hubble parameter, $\tau = 0.09$ the optical depth to reionisation, $A_s = 2.3 \times 10^{-9}$ the scalar perturbation amplitude, $n_s = 0.95$ the scalar spectral index, $\alpha_s = 0$ the running of the scalar index defined at a pivot scale of $k = 0.05$ Mpc^{-1}, and $w = -1$ the dark energy equation of state. The corresponding dark energy density is $\Omega_\Lambda = 0.74$. Note that our definition of N_ν differs from that in [19]. Our definition provides for the possibility of nonstandard radiation density during radiation domination. The definition of [19], on the other hand, counts only the number of massive neutrinos; the effective number of fermionic degrees of freedom during radiation domination is fixed at 3.04.

3. Results

Figure 2 shows the projected 1D marginalised 95 % confidence regions for various parameters within our 8- and 10-parameter models, assuming data from Planck plus different combinations of mock galaxy surveys.

Consider first the 8-parameter model. We note that there is a marked improvement in the projected bounds on $\sum m_\nu$ when galaxy survey data from G1 ($0.5 < z < 2$) and SG ($4 < z < 6$) are combined. This is particularly interesting because the G1 survey has more than twice the effective volume of the SG survey. However, since SG is able to access a higher $k_{\rm max}$ and, being a space-based probe, also suffers from less shot noise, the Planck+G1 and Planck+SG bounds on $\sum m_\nu$ are almost identical. Furthermore, the fact that the underlying LSS spectrum is both scale- and time-dependent (as demonstrated

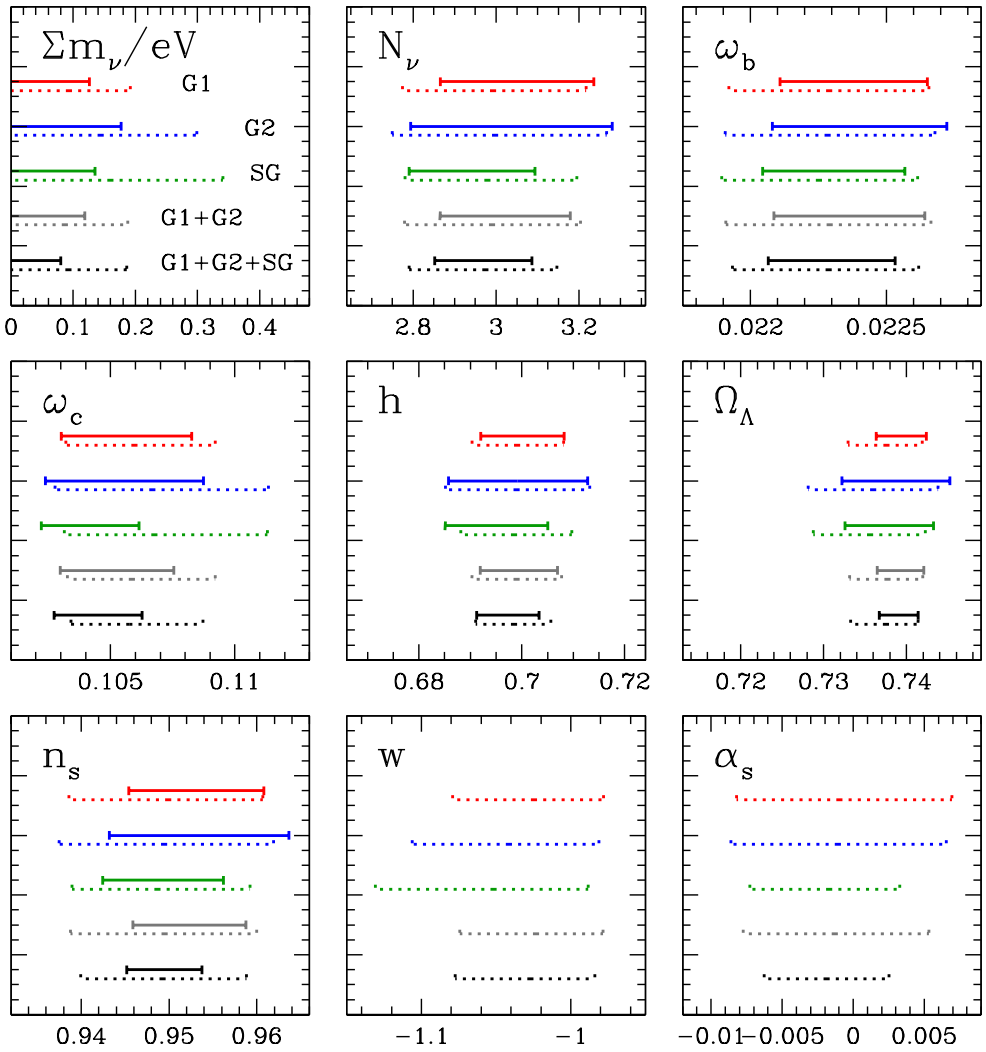

Figure 2. Projected 1D marginalised 95 % confidence regions for various cosmological parameters within the 8- and 10-parameter models, using various combinations of Planck and mock galaxy surveys. In each subplot, the data sets under consideration are, from top to bottom, Planck+G1, Planck+G2, Planck+SG, Planck+G1+G2, and Planck+G1+G2+SG. Solid lines denote constraints in the context of the 8-parameter model, while dotted lines refer to the 10-parameter model.

in Figure 1) means that the G1 and SG mock data sets contain in principle different parameter degeneracies. This can be seen in Figure 2: the SG survey has a better handle on ω_c, N_ν and n_s, while G1 is more constraining for h. Combination of these data sets, therefore, can help lift these degeneracies (even if only partially). Indeed, the combination of G1 and SG yields a bound on $\sum m_\nu$ that is 60 % better than that from G1 or SG alone. A similar trend can also be seen in the allowed regions of n_s, further indicating that we are indeed gaining better shape information from the combination.

This result is particularly noteworthy if we compare it with what can be achieved in a low redshift survey with an effective volume equal to the combined volume of G1

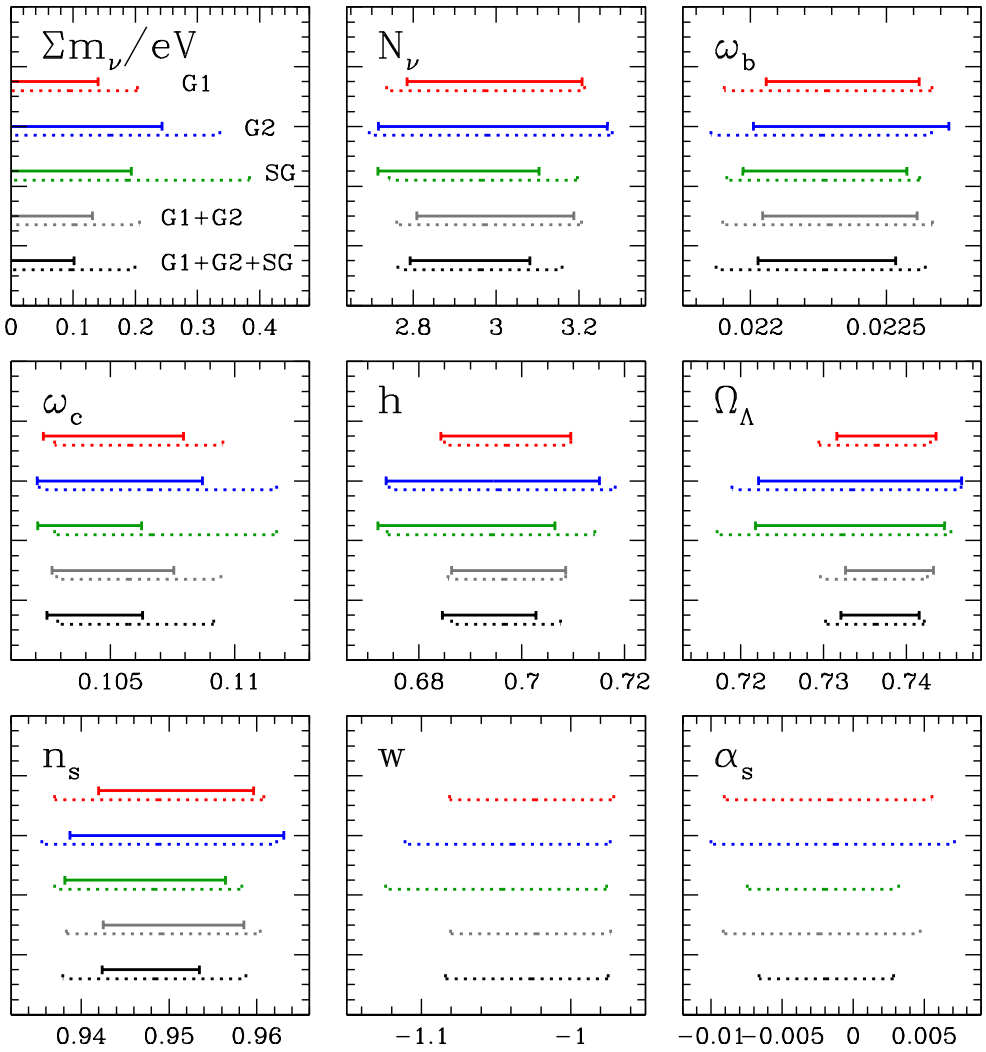

Figure 3. Same as Figure 2, but with power spectrum smoothing as described in section 2.4, i.e., no BAO extraction.

and SG.‡ As an example, we might consider the survey "G1×1.45", which has 1.45 times the effective volume of G1. From volume considerations alone, the improvement in the parameter errors from G1×1.45 relative to G1 is at most a factor of $\sqrt{1.45} \sim 1.2$. But this is a very optimistic figure because the parameter constraints do not depend only on data from galaxy surveys; CMB data, too, play a crucial role, and there is no corresponding increase in the CMB sky coverage. Using an MCMC analysis, we find that Planck+G1×1.45 yields a 95 % upper bound on $\sum m_\nu$ of 0.12 eV. Compared with 0.13 eV from Planck+G1, the actual improvement is negligible and cannot compete with the gain from going to higher redshifts.

For the 10-parameter model, however, the projected sensitivity to $\sum m_\nu$ is much poorer and there is little gain when the SG data set is added to the analysis. In this

‡ Our Planck+G1+G2+SG results include mock data from the G2 survey. However, the bounds come primarily from the combination of G1 and SG. Exclusion of G2 makes virtually no difference.

Table 2. A summary of Figures 2 and 3: projected 1D marginalised 90 % (95 %) upper bounds on $\sum m_\nu$, assuming $\sum m_\nu^{\rm fid} = 0$ (i.e., the "sensitivity").

	8-parameter model		10-parameter model	
Survey	BAO	No BAO	BAO	No BAO
Planck	0.62 (0.73)		0.78 (0.96)	
+G1×5	0.11 (0.13)	0.12 (0.14)	0.17 (0.19)	0.18 (0.20)
+G2	0.15 (0.18)	0.20 (0.24)	0.26 (0.30)	0.30 (0.34)
+SG	0.12 (0.14)	0.17 (0.19)	0.30 (0.34)	0.34 (0.38)
+G1×5+G2	0.10 (0.12)	0.11 (0.13)	0.17 (0.19)	0.18 (0.21)
+G1×5+G2+SG	0.069 (0.080)	0.087 (0.10)	0.16 (0.19)	0.18 (0.20)

model the effect of the neutrino mass can be mimicked by changes in a combination of other parameters, in this case mainly the dark matter density ω_c, the effective number of neutrino species N_ν, the dark energy equation of state w, and the running of the spectral index α_s. The larger k range probed by SG does lead to a better constraint on α_s. Unfortunately this improvement does not translate to the neutrino mass bound.

We caution however that our treatment here, namely, the use of spherically-averaged power spectra instead of two-dimensional spectra with additional geometrical/redshift effects, may not be making full use of the capacity of high-redshift galaxy surveys. Previous studies show that the combination of geometrical effects and BAO can be a very powerful tool to probe separately the Hubble expansion $H(z)$ and the angular diameter distance $D_A(z)$ [24, 25]. This may be useful for breaking the small degeneracy that exists between $\sum m_\nu$ and w.

Figure 3 shows the projected 1D marginalised 95 % confidence regions for the same 8- and 10-parameter models, but now using the smoothed spectra described in section 2.4. Compared with Figure 2, we see that the inclusion of BAO information does lead to better constraints on parameters in general. However, it does not play a role in improving in the neutrino mass bound between Planck+G1+G2+SG and Planck+G1 in the 8-parameter model; the improvement seen in Figure 2 remains intact in Figure 3 even without BAO extraction. Clearly, the improved constraints come from tracing the evolution of the LSS spectral shape.

Lastly, we note the 95 % allowed ranges are in general not centred on the fiducial model because of the non-Gaussian nature of the marginalised posterior distribution. The asymmetric error bars highlight the importance of using MCMC-based forecasts.

3.1. Sensitivity

It is interesting to compare the potential of galaxy redshift surveys to constrain neutrino mass with the expected performance of laboratory experiments such as KATRIN. The sensitivity of KATRIN, defined as the 90 % upper limit assuming a fiducial neutrino mass of zero, is estimated to be 0.2 eV [32]. Derived under the same assumption of

Table 3. Projected 1D marginalised 95 % lower and upper bounds on $\sum m_\nu$ using Planck+G1+G2+SG with BAO extraction for various fiducial $\sum m_\nu$ values.

	8 parameters		10 parameters	
$\sum m_\nu^{\rm fid}$ [eV]	Lower	Upper	Lower	Upper
0.0	0.0	0.080	0.0	0.19
0.050	0.0	0.11	0.0	0.18
0.093	0.027	0.14	0.0	0.21
0.16	0.11	0.20	0.0	0.26
0.19	0.14	0.22	0.10	0.28
0.22	0.18	0.26	0.14	0.31
0.25	0.21	0.28	0.17	0.33
0.28	0.23	0.31	0.21	0.36
0.37	0.32	0.40	0.30	0.44

$\sum m_\nu^{\rm fid} = 0$, Table 2 summarises the projected 90 % and 95 % sensitivities for various combinations of Planck and mock galaxy surveys, with and without BAO extraction, for both the 8- and 10-parameter models.

3.2. Detection threshold

In addition to the sensitivity, KATRIN quotes a detection threshold, defined as the fiducial neutrino mass at which an $N\sigma$ detection is possible. With its present configuration, KATRIN will achieve a 3σ detection of an effective electron neutrino mass of 0.3 eV and 5σ for 0.35 eV [32].

Calculating such a threshold for cosmological data is more involved because it necessitates a scan in fiducial model space. Table 3 and Figure 4 show the results of such a scan; we derive the 1D marginalised 95 % confidence regions using different values of $\sum m_\nu^{\rm fid}$. The projected 95 % detection threshold is then defined as the value of $\sum m_\nu^{\rm fid}$ at which the 95 % lower bound differs from zero.§ In the 8-parameter case the threshold thus defined lies between 0.05 eV and 0.09 eV, whereas in the the 10-parameter model it falls in the range 0.16 eV to 0.19 eV. Comparing these numbers with their corresponding 95 % sensitivities derived in the last section (0.08 eV and 0.19 eV respectively), we see that they are very similar, as one would intuitively expect.

Let us now consider what might be expected from a forecast based on the Fisher matrix, which assumes Gaussianity in the posterior distribution with respect to the model parameters. There are two approaches—and two pitfalls.

First, one can derive σ as function of $\sum m_\nu$, ignoring the fact that the posterior distribution may be non-Gaussian for certain values of $\sum m_\nu$. Besides numerical instabilities (see [23] for a discussion), the σ values derived in this manner, and hence

§ One-tail limits are calculated when the marginalised posterior P drops below 15 % of its maximum at $\sum m_\nu = 0$. This corresponds to $-2\ln P/P_{\rm max} \sim 4$, i.e., roughly 2σ in the case of a Gaussian distribution.

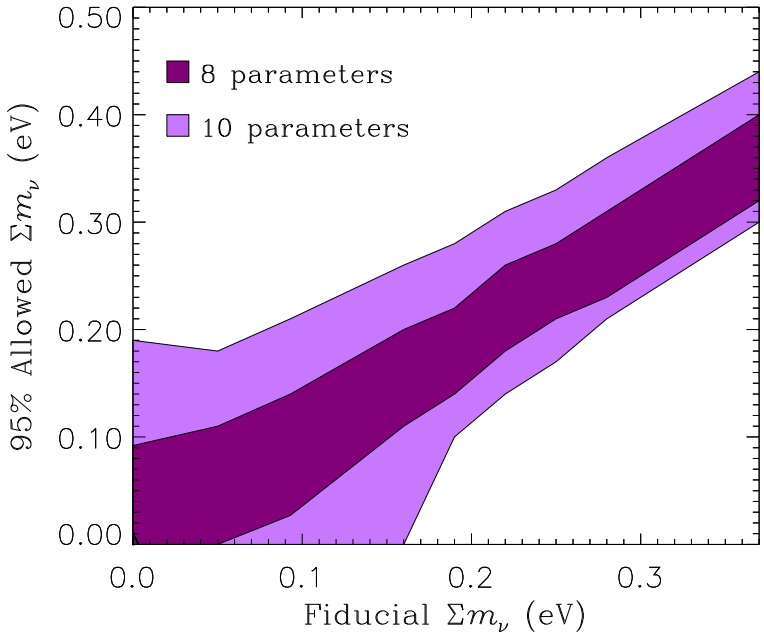

Figure 4. The projected 1D marginalised 95 % confidence range for $\sum m_\nu$ as a function of the fiducial $\sum m_\nu$ for Planck+G1+G2+SG with BAO extraction. The light shaded band denotes the 10-parameter model, while the dark band corresponds to the 8-parameter model.

any confidence regions constructed therefrom, have no meaning in the Bayesian context, simply because the posterior distribution is non-Gaussian.

Alternatively, one may want to avoid the non-Gaussian region by evaluating the Fisher matrix at a larger fiducial value of $\sum m_\nu$ at which the distribution is two-tailed and (hopefully) approximately Gaussian, and then extrapolate the result to other regions of parameter space. For example, in the case of the 10-parameter model, one may want to evaluate the Fisher matrix at, say, $\sum m_\nu = 0.25$ eV. Granting that we can overcome the issue of numerical instability, we should find a "2σ" of approximately 0.08 eV at $\sum m_\nu^{\rm fid} = 0.25$ eV (see Table 3). However, the curvature of the likelihood function is much larger for large values of the fiducial neutrino mass, so that any such estimate of the detection threshold will likely be much too optimistic. Indeed, extrapolating $2\sigma = 0.08$ eV to lower values of $\sum m_\nu^{\rm fid}$, one would be led to conclude that the detection threshold is 0.08 eV, which is clearly much lower than $(0.16 \rightarrow 0.19)$ eV!

This highlights the importance of using MCMC techniques on mock data instead of the Fisher matrix approach in order to get reliable estimates of the potential of future experiments.

4. Conclusions

We have calculated the sensitivity of future CMB probes and LSS measurements from galaxy redshift surveys to the neutrino mass. In particular, we have studied how the measurement of the LSS power spectrum at different redshifts can help to constrain

$\sum m_\nu$ more efficiently than a single, more precise measurement at low redshifts.

Along the same line we also comment on the difference between the sensitivity, the formal upper limit given an underlying neutrino mass of zero, and the detection threshold, the minimum $\sum m_\nu$ measurable at a given confidence level. We have quantified the difference between the sensitivity and the detection threshold in specific cases of CMB+LSS measurements. We suggest that this method is the most reliable for making error forecasts in cosmology. Furthermore, it has the advantage that the results can be directly compared with projected sensitivities and detection thresholds of laboratory experiments such as KATRIN that probe directly the absolute neutrino mass scale.

Within the context of a minimal 8-parameter cosmological model, we find that a minimum neutrino mass of order $0.05 \rightarrow 0.09$ eV can be detected at 95 % confidence level using Planck and a combination of low and high redshift galaxy surveys, while the 95 % sensitivity is 0.08 eV. The latest neutrino oscillation data prefer the mass splittings $\Delta m^2_{12} \sim 8 \times 10^{-5}$ eV^2 and $\Delta m^2_{23} \sim 2.5 \times 10^{-3}$ eV^2 [33, 34]. If the lightest eigenstate has zero mass, these mass splittings imply $\sum m_\nu \simeq 0.06$ eV for the normal hierarchy and 0.1 eV for the inverted hierarchy. With the survey configurations chosen for our study, it will not be possible to differentiate definitively between the two hierarchy schemes. In more complex cosmological models the detection threshold and sensitivity become even worse. In the concrete case shown in Table 3, the sensitivity worsens by a more than a factor of two, while the increase in the detection threshold is threefold so that a positive detection will only be possible if neutrino masses are in the quasi-degenerate regime.

We note that the survey configurations employed in our analysis are not necessarily overly optimistic. A very recent study of neutrino mass measurements from Planck plus a future wide-field galaxy survey out to $z \sim 2$ [35] assumes a much larger effective survey volume than our G1 survey (roughly comparable to G1×12). We have checked explicitly that the 95 % sensitivity to $\sum m_\nu$ in this case is 0.06 eV for the 8-parameter model, a figure that can almost be matched by our 0.08 eV from a combination of low- and high-redshift measurements with a much smaller total survey volume.

Finally we stress that although future high-redshift galaxy surveys will be extremely useful for probing small neutrino masses, they are by no means the only source of information about the LSS power spectrum. Weak gravitational lensing of distant galaxies, for example, will provide a complementary and possibly even more sensitive probe of neutrino properties [12–15]. In the more distant future, surveys of the 21-cm line from beyond the epoch of reionisation will provide access to the matter power spectrum at even higher redshifts.

Acknowledgements

We acknowledge computing resources from the Danish Center for Scientific Computing (DCSC). SH acknowledges support from the Alexander von Humboldt Foundation through a Friedrich Wilhelm Bessel Award, and thanks the Max-Planck-Institut für

Physik for hospitality during the initial stages of this work. YYYW thanks Jan Hamann for useful discussions and suggestions.

References

[1] A. Goobar, S. Hannestad, E. Mortsell and H. Tu, JCAP **0606** (2006) 019 [arXiv:astro-ph/0602155].
[2] U. Seljak, A. Slosar and P. McDonald, JCAP **0610** (2006) 014 [arXiv:astro-ph/0604335].
[3] B. Feng, J. Q. Xia, J. Yokoyama, X. Zhang and G. B. Zhao, JCAP **0612** (2006) 011 [arXiv:astro-ph/0605742].
[4] M. Cirelli and A. Strumia, JCAP **0612** (2006) 013 [arXiv:astro-ph/0607086].
[5] S. Hannestad and G. G. Raffelt, JCAP **0611** (2006) 016 [arXiv:astro-ph/0607101].
[6] G. L. Fogli *et al.*, arXiv:hep-ph/0608060.
[7] D. N. Spergel *et al.*, arXiv:astro-ph/0603449.
[8] M. Tegmark *et al.*, Phys. Rev. D **74** (2006) 123507 [arXiv:astro-ph/0608632].
[9] C. Zunckel and P. G. Ferreira, arXiv:astro-ph/0610597.
[10] J. R. Kristiansen, O. Elgaroy and H. Dahle, arXiv:astro-ph/0611761.
[11] J. Lesgourgues and S. Pastor, Phys. Rept. **429** (2006) 307 [arXiv:astro-ph/0603494].
[12] A. R. Cooray, Astron. Astrophys. **348** (1999) 31 [arXiv:astro-ph/9904246].
[13] K. N. Abazajian and S. Dodelson, Phys. Rev. Lett. **91** (2003) 041301 [arXiv:astro-ph/0212216].
[14] Y. S. Song and L. Knox, Phys. Rev. D **70** (2004) 063510 [arXiv:astro-ph/0312175].
[15] S. Hannestad, H. Tu and Y. Y. Y. Wong, JCAP **0606** (2006) 025 [arXiv:astro-ph/0603019].
[16] W. Hu, D. J. Eisenstein and M. Tegmark, Phys. Rev. Lett. **80** (1998) 5255 [arXiv:astro-ph/9712057].
[17] S. Hannestad, Phys. Rev. D **67** (2003) 085017 [arXiv:astro-ph/0211106].
[18] J. Lesgourgues, S. Pastor and L. Perotto, Phys. Rev. D **70** (2004) 045016 [arXiv:hep-ph/0403296].
[19] M. Takada, E. Komatsu and T. Futamase, Phys. Rev. D **73** (2006) 083520 [arXiv:astro-ph/0512374].
[20] K. Glazebrook, D. Eisenstein, A. Dey and B. Nichol, arXiv:astro-ph/0507457.
[21] G. J. Hill, K. Gebhardt, E. Komatsu and P. J. MacQueen, AIP Conf. Proc. **743** (2004) 224.
[22] `http://www.cfa.harvard.edu/cip/`
[23] L. Perotto, J. Lesgourgues, S. Hannestad, H. Tu and Y. Y. Y. Wong, JCAP **0610** (2006) 013 [arXiv:astro-ph/0606227].
[24] H. J. Seo and D. J. Eisenstein, Astrophys. J. **598** (2003) 720 [arXiv:astro-ph/0307460].
[25] W. Hu and Z. Haiman, Phys. Rev. D **68** (2003) 063004 [arXiv:astro-ph/0306053].
[26] A. Lewis and S. Bridle, Phys. Rev. D **66** (2002) 103511 [arXiv:astro-ph/0205436].
[27] `http://cosmologist.info`
[28] M. Tegmark, Phys. Rev. Lett. **79** (1997) 3806 [arXiv:astro-ph/9706198].
[29] W. J. Percival *et al.*, arXiv:astro-ph/0608635.
[30] `http://astro.estec.esa.nl/SA-general/Projects/Planck/`
[31] `http://www.rssd.eas.int/Planck`
[32] G. Drexlin [KATRIN Collaboration], Nucl. Phys. Proc. Suppl. **145** (2005) 263.
[33] A. Y. Smirnov, arXiv:hep-ph/0702061.
[34] M. Maltoni, T. Schwetz, M. A. Tortola and J. W. F. Valle, New J. Phys. **6** (2004) 122 [arXiv:hep-ph/0405172].
[35] F. B. Abdalla and S. Rawlings, arXiv:astro-ph/0702314.